Journal of Bacteriology
July 2010 ; Volume 192 (14) : Pages 3689-3698
http://dx.doi.org/10.1128/JB.00268-10

Structure-Specific Nuclease Activities of *Pyrococcus abyssi* RNase HII

Sébastien Le Laz[1], Audrey Le Goaziou[1, 2] and Ghislaine Henneke[1, 2, *]

[1] Université de Bretagne Occidentale, UMR 6197, Laboratoire de Microbiologie des Environnements Extrêmes, 29280 Plouzané, France
[2] Ifremer, UMR 6197, Laboratoire de Microbiologie des Environnements Extrêmes, BP 70, 29280 Plouzané, France

*: Corresponding author : Ghislaine Henneke, email address : Phone: 33 2 98 22 46 09. Fax: 33 2 98 22 47 57, email address : ghenneke@ifremer.fr

Abstract:

Faithful DNA replication involves the removal of RNA residues from genomic DNA prior to the ligation of nascent DNA fragments in all living organisms. Because the physiological roles of archaeal type 2 RNase H are not fully understood, the substrate structure requirements for the detection of RNase H activity need further clarification. Biochemical characterization of a single RNase H detected within the genome of *Pyrococcus abyssi* showed that this type 2 RNase H is an Mg- and alkaline pH-dependent enzyme. *Pab*RNase HII showed RNase activity and acted as a specific endonuclease on RNA-DNA/DNA duplexes. This specific cleavage, 1 nucleotide upstream of the RNA-DNA junction, occurred on a substrate in which RNA initiators had to be fully annealed to the cDNA template. On the other hand, a 5' RNA flap Okazaki fragment intermediate impaired *Pab*RNase HII endonuclease activity. Furthermore, introduction of mismatches into the RNA portion near the RNA-DNA junction decreased both the specificity and the efficiency of cleavage by *Pab*RNase HII. Additionally, *Pab*RNase HII could cleave a single ribonucleotide embedded in a double-stranded DNA. Our data revealed *Pab*RNase HII as a dual-function enzyme likely required for the completion of DNA replication and DNA repair.

INTRODUCTION

DNA replication in all living organisms takes place concurrently on two separate strands. The lagging strand consists of multiple discontinuous segments called Okazaki fragments, whereas the leading strand comprises one large continuous segment. Production of each individual lagging strand by DNA polymerase is primed by a short stretch of RNA. Later on, these RNA primers are eliminated and the resulting gap is filled with deoxyribonucleotides prior to ligation. Priming and DNA elongation at the replication fork involve a set of specialized polymerising enzymes which differ from replicative DNA polymerases, and one another, to correct erroneously inserted nucleotides. In archaeal cells, the priming complex lacks proofreading 3'-5' exonuclease activity (13, 14) present in the replicative DNA polymerases B and D (1, 8). Consequently, mismatches in the vicinity of the RNA-DNA junction could arise in replicating cells, as already observed in eukaryotes (28, 31). Similarly, single ribonucleotides incorporated during DNA replication (20, 26) or by external agents (32) would represent another source of erroneous nucleotides. Persistence of residual RNA during DNA replication would be detrimental for the cells, suggesting that a combination of specific and efficient nucleolytic processes is absolutely required to preserve DNA integrity.

Ribonucleases H (RNase H) are enzymes which degrade the RNA portion of RNA/DNA or RNA-DNA/DNA duplexes (29). RNases H are classified into two major families, type 1 and type 2, based on amino acid sequence (21). The type 1 family includes bacterial RNase HI, mammalian RNase HII, the RNase H domain of reverse transcriptase and archaeal RNase HI and the type 2 contains bacterial RNase HII and RNase HIII, mammalian RNase HI and archaeal RNase HII (21). While type 2 RNase H enzymes are universally conserved in the three domains of life, their physiological role remains elusive. Much less is known about the type 2 family compared to the type 1 RNase H enzymes. The multiplicity of RNases H within

66 a single cell complicates the situation, although presumable roles in DNA replication, DNA
67 repair and transcription have been assigned as recently reviewed (2, 30). In archaea, structural
68 and biochemical characterization of type 2 RNases H (3, 4, 10, 12, 16, 19) suggested they can
69 initiate RNA removal from DNA duplexes, based on their ability to specifically cleave 5' to
70 the junctional ribonucleotide. However, despite this information, the physiological role of
71 type 2 RNases H still remains elusive. They could be involved in the completion of either
72 leading or lagging strands or both. Additional biochemical experiments with catalytic
73 intermediates should provide valuable knowledge on the participation of these archaeal
74 cellular enzymes at the replication fork and in DNA repair.
75 To investigate this question, we have designed a set of RNA/DNA duplex, cognate RNA-
76 DNA/DNA duplex (15), a single ribonucleotide embedded in a DNA duplex (DNA-1RNA-
77 DNA/DNA) as substrates, and employed type 2 RNase H from the hyperthermophilic deep-
78 sea euryarchaeon *Pyrococcus abyssi (Pab)*, *Pab*RNase HII. Since a single *rnh* gene exists in
79 the genome of *P. abyssi* (6), RNase HII is likely the key enzyme involved in RNA elimination
80 in this organism. Thus, *Pab*RNase HII can be considered as the representative of type 2
81 RNase H.
82 Here, we analysed the cleavage specificity of *Pab*RNase HII for substrates with Okazaki
83 fragment-like structure. We also tested *Pab*RNase HII activity on Okazaki fragment-like
84 substrates in the presence of mismatched base pair in order to assess the molecular
85 mechanism of recognition of the RNA-DNA junction and the subsequent cleavage specificity.
86 In addition, we examined whether *Pab*RNase HII can incise the DNA backbone on the 5'-side
87 of a single ribonucleotide embedded in a DNA duplex. Our data provide substantial evidences
88 that the single RNase H in *P. abyssi* has a dual role in maintenance of genome integrity. The
89 results from this study are further discussed to define potent roles of type 2 RNase H from *P.*

90 *abyssi* in the resolution of RNA fragments at the replication fork and in the repair of single
91 embedded ribonucleotides.

MATERIALS AND METHODS

Nucleic acid substrates.

Gel-purified oligonucleotides for preparing the substrates for RNase HII assays were purchased from Eurogentec (Belgium) and their sequences are listed in Table 1. Fluorescent labelling at the 5'- end was performed with the 5' End Tag kit labelling system from Vector Laboratories (California). Free fluorescent dyes were removed on MicroSpinTM G-25 columns. For some experiments, 5'-end- or 3'-end-fluorescent labelled oligonucleotides were chemically synthesized and HPLC-purified by Eurogentec (Belgium). To generate the substrates for the RNase HII assays, the appropriate oligonucleotides were mixed in 1:1 molar ratio in 20 mM Tris–HCl (pH 7.4), 150 mM NaCl, heated to 75°C and slowly cooled to room temperature.

Cloning, production and purification of *Pab*RNase HII.

The gene encoding *Pab*RNase HII (PAB0352) was cloned into the pQE-80L expression vector (Qiagen). *Pab*RNase HII was overexpressed in *E. coli* strain BL21-CodonPlus-RIL strain (Stratagene) as a histidine-tagged protein and purified to near homogeneity via Ni-NTA beads (Qiagen) and S200 gel filtration using fast protein liquid chromatography (GE Healthcare) as previously described (16). Protein integrity was analyzed by MALDI-TOF analyses (Innova Proteomics, France). *Pab*RNase HII purity was controlled by SDS–PAGE gradient gel (4-20 %) electrophoresis (Thermo Scientific).

Amino acid sequence alignments and secondary structure.

Amino acid sequence alignments have been constructed by ClustalW2 (available at www.ebi.ac.uk/clustalW2/). Secondary structure elements calculated with the program

ESPript 2.2 (available at http://espript.ibcp.fr/ESPript/ESPript/) refer to the structure of *Tko*KOD1RNase HII (PDB: 1IO2).

Assays for RNase HII activity.

Assays to monitor cleavage by *Pab*RNase HII were performed in RNase HII buffer (10 µl) containing: 50 mM Tris-HCl (pH 8), 5 mM dithiothreitol, 5 mM $MgCl_2$ and 50 nM of DNA substrates. Enzymes were diluted from concentrated stocks in 20 mM Tris-HCl (pH 7.5), 20 % glycerol prior to usage. Enzyme concentrations for a typical reaction ranged from 4 to 400 nM, unless otherwise specified. After addition of *Pab*RNase HII, reactions were incubated at 60°C for 30 minutes and stopped on ice with 15 µl of stop buffer (98 % formamide, 10 mM EDTA). Samples were heated at 95°C for 5 minutes. A base hydrolysis ladder was prepared by incubation of the labelled RNA-DNA strand (10 µM) with snake venom phosphodiesterase I (0.018 units) for 10 minutes at 37°C. Product analysis was carried out by electrophoresis on 15 % denaturing polyacrylamide gels. After visualisation with a Mode Imager Typhoon 9400 (GE Healthcare), quantification of the results was performed using ImageQuant 5.2 software. In all cases, the percentage of substrate hydrolysis was determined by the products / (products + substrate) ratio, allowing a correction for loading errors and a comparison of cleavage efficiency irrespective of the different products generated.

To analyse divalent cations or pH dependence, RNase HII assays were carried out with 50 nM of *Pab*RNase HII and 50 nM of the S1 substrate at 60°C for 30 min. Data are the average of triplicate measurements and are shown with standard deviations (SD).

To determine the kinetic parameters, steady-state kinetic reactions were carried out in the same conditions as described above by using substrate 1 at concentrations ranging from 0.03 to 3 µM. Initial velocity experiments were monitored as a function of time with 60 nM of *Pab*RNase HII at 60°C such that the rate of converted substrate did not exceed 20 % of the

142 total. Velocity measurements were reported as the amount of hydrolysed substrate (μM) over
143 time (min). The observed rates of converted substrates with *Pab*RNase HII were firstly
144 determined from Lineweaver-Burk plots. The data were fit by nonlinear regression using the
145 Marquardt-Levenberg algorithm (EnzFitter 2.0, BioSoft) to the Michaelis-Menten equation.
146 Kinetic parameters, *K*m and *V*max, were obtained from the fit and were used to calculate the
147 catalytic efficiency (k_{cat}/K_m) of *Pab*RNase HII. The kinetics values are the average of at least
148 triplicate determinations and are shown with standard deviations (SD). Any adjustments to the
149 above are noted in the Figure Legends.

RESULTS

Archaeal RNase HII homologues

*Pab*RNase HII showed amino acid sequence similarities of 75.2 % with *Tko*RNase HII, and 65 % with *Afu*RNase HII. Analysis of protein primary structures and related secondary structures outlined subtle differences between the three proteins (Fig. 1A). On the one hand, *Pab*RNase HII and *Afu*RNase HII are isoelectric at basic pH (isoelectric point values of 9 and 7.6, respectively), whereas *Tko*RNase HII is isoeletric at acidic pH (isoelectric point of 5.5). On the other hand, *Pab*RNase HII, *Tko*RNase HII and *Afu*RNase HII exhibit conserved secondary structure elements, with the exception that the α9-helix is incomplete in *Afu*RNase. This secondary structure element is important for *Tko*RNase HII to bind the substrate (19). Structural alignments resulted in the identification of conserved active site residues (Asp7, Glu8, Asp105 and Asp135) in *Pab*RNase HII, suggesting a similar catalytic mechanism between the three enzymes.

Enzymatic properties of *P. abyssi* RNase HII

His-tagged *Pab*RNase HII was overproduced in *E. coli* and purified to give a single band on SDS-PAGE (Fig. 1B, lane 2). Reactions were carried out at 60 °C, the optimum temperature for *Pab*RNase HII activity (16). *Pab*RNase HII was assayed under different pH and ionic conditions, varying both the nature and the concentration of divalent cations, according to the general procedure described in Materials and methods using the RNA-DNA/DNA substrate (S1). The optimum pH for its activity was observed between pH 8.0 and 8.5 (Fig. 1C). However, at pH 7.5 and 9, the enzyme retained about 60 % of the activity measured at pH 8.

175 *Pab*RNase HII exhibited enzymatic activity in the presence of $MgCl_2$, $MnCl_2$ and $CoCl_2$ (Fig.
176 1D). While *Pab*RNase HII activity was entirely dependent on the presence of a divalent
177 cation, the enzyme was not active in the presence of $NiCl_2$, $FeCl_2$, $ZnCl_2$, $CaCl_2$ or $CuSO_4$.
178 The most preferred metal ion for *Pab*RNase HII was $MgCl_2$ but the $MnCl_2$ and $CoCl_2$ could
179 substitute for the $MgCl_2$ with reduced cleavage activity. As shown in Fig. 1D, the metal
180 concentrations which gave the highest enzymatic activity were 5 mM for $MgCl_2$, and 2 mM
181 for $MnCl_2$ and $CoCl_2$. Substrate hydrolysis in the presence of 5 mM for $MgCl_2$ was 1.5- and
182 3.2- fold higher than those determined at 2 mM for $MnCl_2$ and $CoCl_2$, respectively.
183 The kinetic parameters of *Pab*RNase HII were determined in the presence of RNA-
184 DNA/DNA substrate (S1) and 5 mM $MgCl_2$. The results are summarized in Table 2 and
185 compared to that of type 2 RNase H archaeal homologue from *Archaeoglobus fulgidus*
186 (*Afu*RNase HII) as already described (4). Interestingly, *Afu*RNase HII showed stronger
187 substrate binding affinity than *Pab*RNase HII, as attested by a 10-fold lower K_m value, while
188 the catalytic rate constants of the two enzymes were similar (Table 2). As a consequence,
189 *Pab*RNase HII displayed a lower catalytic efficiency on RNA-DNA/DNA substrate as
190 compared to *Afu*RNase HII (Table 2).
191
192 **Ribonuclease activity of *P. abyssi* RNase HII**
193
194 Firstly, we examined whether *Pab*RNase HII could cleave the RNA strand of a RNA/DNA
195 duplex (S11). As shown in Fig. 2, different 5'-terminal RNA products accumulated depending
196 on the enzyme concentration, indicating that *Pab*RNase HII exhibited endoribonuclease
197 activity. Because control assays without enzyme showed background degradation of the RNA
198 primer (Fig. 2A, lane 2), they were subtracted from cleavage products signal. Less than 19 %
199 intact RNA was present upon incubation with 100 nM *Pab*RNase HII for 30 min at 60°C (Fig.

2A, lane 6). Multiple cleavage sites were detected (Fig. 2A, lanes 2-8) and comparative analysis of products with those from the snake venom phosphodiesterase digest of 5'-end labelled 32 nucleotide (nt) RNA ladder (Fig. 2A, lane 1) pointed out main cleavage events (6-, 8-, 9-, 12-, 13- and 17-nt). Moreover, further processing of short RNA fragments could be observed by increasing enzyme concentrations. It is important to note that *Pab*RNase HII used in this study did not exhibit nuclease activity on single-stranded RNA (Fig. 2B). All together, these results provided evidence that *Pab*RNase HII acts as an endoribonuclease on RNA/DNA duplexes.

Structure-specific cleavage activities in *P. abyssi* RNase HII

The absence of cleavage specificity of RNA/DNA duplexes prompted us to look for digestion of other relevant physiological substrates. We hypothesize that *Pab*RNase HII participates in the mechanism of RNA primer removal, an activity which can occur once at the leading strand or much more frequently at the lagging strand. Therefore, we explored the cleavage specificity of *Pab*RNase HII for substrates with Okazaki fragment-like intermediates.

PabRNase HII specifically cleaves RNA-initiated DNA segments fully annealed to a DNA template

We initially began to examine whether *Pab*RNase HII could hydrolyse a cognate double-stranded Okazaki fragment (15). A single strand composed of 12 nucleotides of RNA (RNA12nt) followed by 18 nucleotides of DNA (DNA18nt), fluorescently labelled at the 5'-end, was annealed to a complementary 30 nucleotides DNA template to form the S1 substrate as shown in Fig. 3A. When this substrate was incubated in the presence of increasing *Pab*RNase HII amounts, a major product appeared (Fig. 3B, lanes 2-5). This oligomer was

shown to correspond to 11 nucleotides RNA by migration with respect to a snake venom phosphodiesterase-generated digest of RNA12ntDNA18nt (Fig. 3B, lane 1). In addition to this main cleavage site, minor cleavage sites characteristic of non-specific nuclease activity were also found throughout the length of the RNA (Fig. 3B, lanes 2-5). Over time, *Pab*RNase HII activity released the same oligomer which was basically free of any additional shorter fragments, suggesting that this product was not transiently formed and prevailed during the reaction (data not shown). Interestingly, *Pab*RNase HII did not hydrolyse single-stranded RNA12ntDNA18nt (Fig. 3B, lanes 6-9) indicating that cleavage is dependent on the heteroduplex structure. It is of note that the pale band at ~9-nt present at relatively constant levels did not correspond to a specific cleavage product (Fig. 3B, lanes 2-9). Absence of specific cleavage was also observed with substrates lacking the complementary DNA template to either the RNA12nt or the DNA18nt sequence (data not shown). While a fully annealed RNA12ntDNA18nt/DNA is definitely required to detect cleavage specificity, *Pab*RNase HII did not hydrolyse the complementary DNA template (Fig. 3B, lanes 10-13). Shorter bands were not due to cleavage activity since they were detectable in all lanes with equal intensities even in the absence of enzyme. These data demonstrated that *Pab*RNase HII can act endonucleolytically on initiator RNA and displays a specific cleavage activity dependent on the heteroduplex structure.

PabRNase HII specifically cleaves the fully annealed RNA strand of Okazaki fragment-gapped intermediates but not a 5'-RNA flap

Both at the leading and lagging strands, sequential enzymatic steps are thought to be part of the RNA primer elimination mechanism in *P .abyssi*. As a consequence, diverse structural Okazaki fragment-like substrates would arise. Therefore, we examined whether structural intermediates (S4, S5 and S6) which can be captured during the process (outlined in Fig. 4A)

could direct the cleavage activity of *Pab*RNase HII. On the 40-gapped S4 intermediate composed of an upstream DNA primer and a downstream RNA-DNA fragment fully annealed to the complementary DNA template, *Pab*RNase HII specifically cleaved the RNA segment, releasing one ribonucleotide attached to the DNA segment (Fig. 4B, lanes 1-4). During the elongation step, the size of the gap would decrease to reach the next RNA initiator. By reconstitution of model transient substrates, we demonstrated that both the 20-nt gapped S5 intermediate (Fig. 4B, lanes 5-8) and a nicked intermediate (data not shown) were specifically cleaved. Collectively, cleavage efficiencies of the gapped and nicked Okazaki fragment intermediates were comparable to those of double-stranded RNA-DNA fragments (Fig. 3B, lanes 2-5). However, on a 5'-RNA flap which can result from strand displacement activity by *Pab*polD of the next Okazaki fragment (11), *Pab*RNase HII did not significantly release oligomers (Fig. 4B, lanes 9-12). It is of note that a faint intensifying band at 8-nt (Fig. 4B, lanes 9-12) did not correspond to a specific cleavage product. These results clearly indicated that *Pab*RNase HII is not involved in the cleavage of single-stranded RNA initiator despite the presence of surrounding DNA duplexes. These data are consistent with our observations from Fig. 3B that *Pab*RNase HII exclusively cuts double-stranded RNA-DNA/DNA substrates. Importantly, we demonstrated that *Pab*RNase HII cleaves the RNA initiator fully annealed to the complementary DNA template independently of the size of the gap. In addition, we provided evidence that a 5'-RNA flap is not an appropriate substrate for *Pab*RNase HII, suggesting the requirement of additional enzymes to fully ensure the removal of Okazaki fragment intermediates at the lagging strand.

PabRNase HII specifically cuts the RNA-DNA/DNA when the RNA is completely annealed to the DNA template

The above results indicated that *Pab*RNase HII specifically cleaves the RNA in an RNA-DNA/DNA duplex one ribonucleotide upstream of the RNA-DNA junction. Based on this observation, we attempted to gain further information about the structure-specific recognition of the RNA-DNA junction. We predicted that mismatches located either downstream or upstream of the site of cleavage would alter the structure of the junction and prevent *Pab*RNase HII from recognising and cutting the substrate. Such substrates, which can be created during priming and DNA synthesis in eukaryotes (28, 31), could also be relevant in *P. abyssi* cells. In particular, the priming heterodimeric polymerase in *P. abyssi*, *Pab*p46/41 complex, does not possess 3'-5' exonucleolytic activity and can consequently misincorporate nucleotides, creating mismatched base pairs at or near the RNA-DNA junction.

The complementary DNA template was designed to produce specific mismatches with the RNA12ntDNA18nt strand (Fig. 5A). When the mismatch was the deoxynucleotide downstream of the site of cleavage, *Pab*RNase HII efficiently cleaved the S7 substrate and cut at one site into the RNA segment, leaving a monoribonucleotide attached to the DNA18nt strand (Fig. 5B, lanes 2-5). Cleavage efficiencies were still comparable to those of model Okazaki fragments described above. This result seems to point out that a deoxynucleotide mismatched Okazaki fragment does not affect recognition and specific cleavage by *Pab*RNase HII. We next considered that ribonucleotide mismatches positioned downstream (Fig. 5A, S8 substrate) or upstream (Fig. 5A, S9 substrate) of the cutting site would be crucial for directing the cleavage specificity of *Pab*RNase HII. Interestingly, the presence of the ribonucleotide just downstream of the cutting site induced random endonucleolytic cleavage with predominant products (Fig. 5B, lanes 6-9 and Fig. 5C, S8 substrate) and the percent of hydrolysed products was equivalent to that of Okazaki fragment-like substrates. When the ribonucleotide mismatch was positioned upstream of the site of cleavage, random endonucleolytic activity was enhanced but cleavage efficiencies were lowered (Fig. 5B, lanes

10-13). Multiple cleavage sites due to the loss of specificity appeared (Fig. 5C, S9 substrate). Taken together these data showed for the first time that an archaeal RNase HII requires complete hybridization of the RNA segment to the DNA template in order to confer specific cleavage of RNA-DNA/DNA duplexes.

PabRNase HII specifically cuts a single embedded ribonucleotide in a DNA duplex

We anticipated that *Pab*RNase HII nuclease could act on a single ribonucleotide embedded in DNA. A single ribonucleotide in a DNA duplex could arise via misincorporation of ribonucleotide during DNA synthesis or by ligation of the monoribonucleotide attached to the DNA after cleavage of Okazaki fragments by type 2 RNase H (26). To determine whether an embedded ribonucleotide in DNA (S10 substrate) is a hydrolysable substrate, endonuclease activity of *Pab*RNase HII was carried out. Fig. 6B, lanes 8-11 demonstrated that *Pab*RNase HII was able to recognise and to cleave endonucleolytically on the 5'-side of an embedded monoribonucleotide. Additional fragments, shorter than the released 11-nt, were faintly detectable. Basically, cleavage efficiencies of a single embedded ribonucleotide were similar to those of model Okazaki fragment S1 substrate (Fig. 6B, compare lanes 2-5 and lanes 8-11). Overall, we showed that *Pab*RNase HII is active on single embedded ribonucleotides in a DNA duplex and releases a major product consisting of a single ribonucleotide on the 5'-end of the downstream DNA segment.

DISCUSSION

Two types of RNase H, type 1 and type 2, have been identified in a multiplicity of archaeal genomes. While most archaeal microorganisms have only one type of RNase H, a few archaea such as *Sulfolobus tokodaii* and *Haloferax volcanii* possess both types of RNase H. Although the physiological significance of multiple *rnh* genes in single archaeal genomes is not well understood, RNases H are thought to be involved in important cellular processes (3, 10, 16, 23, 24). Interestingly, archaeal type 2 RNase H appears more universal because the encoding gene is distributed in almost all archaeal genomes. Sequence comparison within archaeal type 2 RNases H revealed a high degree of sequence similarity with conserved active site residues, suggesting that these enzymes may have common biochemical properties (3, 9). In this report, we demonstrated that *Pab*RNase HII, type 2 RNase H from *P. abyssi,* is as an alkaline enzyme. This property seems to be a hallmark of type 2 thermostable RNases H (3, 9, 22). In addition, *Pab*RNase HII appeared to prefer the Mg^{2+} ion for RNase activity rather than Mn^{2+} or Co^{2+}. Distinct metal dependencies have been described for *Archaeoglobus fulgidus* and *Thermococcus kodakaraensis KOD1* RNase HII with Mn^{2+}- or Co^{2+}-preference, respectively (3, 9). Metal ion usage by archaeal RNases HII may be a consequence of the environmental conditions they thrive. It may also dictate the substrate requirement for hydrolysis and confer a specialised function to the enzyme in the maintenance of genome integrity. Determination of kinetic parameters highlighted that the homologous archaeal enzymes, *Afu*RNase HII and *Pab*RNase HII, showed distinct catalytic efficiencies for RNA-DNA/DNA substrates. These results mainly reflected differences in substrate binding affinity. In general, biochemical discrepancies observed between the three enzymes are possibly related to variations in secondary structure elements and physicochemical parameters (e.g., isoelectric point). Despite these subtle differences, archaeal RNase HII seem to possess conserved structural features

required to specifically recognise a comparable region of the substrates, and to produce similar products. Like other type 2 archaeal RNase H, *Pab*RNase HII behaved as an efficient endoribonuclease on RNA/DNA duplexes, stalling at particular sites (3, 9). Moreover, most of the biochemical features of *Pab*RNase HII overlapped those of the eukaryotic equivalent, type 2 RNase H, described as a key enzyme in Okazaki fragment processing (17).

With diverse constructs representing replication-fork intermediates, *Pab*RNase HII made structure-specific endonucleolytic cleavage in the RNA initiator, leaving a single ribonucleotide at the 5'-end of the RNA-DNA junction. Cleavage 5' to the junctional ribonucleotide required the presence of double-stranded substrates with the RNA segment fully annealed to the complementary strand. Gapped double-stranded substrates containing RNA-DNA junctions did not alter cleavage specificity. However, a single-stranded 5'-RNA flap was resistant to cleavage activity, indicating that *Pab*RNase HII does not carry out this reaction at the replication fork. On the other hand, other results have demonstrated that the structure-specific nuclease, Flap endonuclease I (Fen I), can cleave substrates with RNA flap structures, bypassing the need for Rnase HII in Okazaki fragment processing.(18, 27). Furthermore, we demonstrated that mismatches in the RNA portion, produced by erroneous priming and polymerising activities during initiation of DNA replication in eukaryotes (28, 31), resulted in loss of specificity by *Pab*RNase HII. These results demonstrate, for the first time, that the RNA residues in the vicinity of the RNA-DNA junction are key structural determinants for cleavage specificity of type 2 archaeal RNase H. Notably, archaeal type 2 RNase H seems to differ from eukaryotic type 2 (17) in that it recognizes the RNA strand rather than the RNA-DNA junction. Possibly, the RNA portion of the RNA-DNA junction annealed to DNA template adopts an intermediate helical structure, which might target RNase HII recognition and induce specific cleavage. This hypothesis is sustained by the observation that RNA/DNA and DNA/DNA duplexes form A-type and B-type helices, respectively (5, 7).

We recently proposed a model of DNA replication in *P. abyssi* that involves the family B DNA polymerase, *Pab*polB, at the leading strand and the family D DNA polymerase, *Pab*polD, at the lagging strand (11). This model is reinforced by complementary studies demonstrating that *Pab*polB is likely the leading strand DNA polymerase (25). Typically, *Pab*polD has the capacity to displace the downstream fragment including the RNA initiator, while *Pab*polB is not active on this substrate. In this situation, RNA-initiated DNA segments fully annealed to a DNA template would arise only at the leading strand. Because *Pab*RNase HII cannot cleave 5'-RNA flap templates, *Pab*RNase HII would recognize the annealed RNA primer at the leading strand and promotes its endonucleolytic cleavage. The resulting 5' phosphorylated junction ribonucleotide attached to the DNA would be subsequently displaced by *Pab*polB and cleaved by *Pab*Fen I, prior to ligation by *Pab*DNA ligase I. Thus, the functional importance of RNase HII in the completion of leading strand DNA replication in *P. abyssi* awaits the *in vitro* reconstitution of this multi-step enzymatic process (manuscript in preparation). Despite common biochemical properties with the eukaryotic type 2 RNase H, single archaeal RNases HII could be cellular enzymes involved in the removal of RNA residues at the leading strand rather than at the lagging strand. Such biological assumptions would indicate that these microorganisms have evolved differently by targeting analogous enzymes to unrelated biological functions.

Moreover, we demonstrated that *Pab*RNase HII is able to cleave at the 5'-end of single embedded ribonucleotides with similar efficiency as at cognate Okazaki fragments (15). Since such structural substrates can appear *in vivo* during Okazaki fragment processing from intrinsic RNA ligation activity or erroneous nucleotide incorporation (26) and during exposure to external damaging agents (32), we suggest that *Pab*RNase HII can participate in the removal of inappropriate ribonucleotides from the hyperthermophilic chromosome. These biochemical characteristics would imply that *Pab*RNase HII promotes the initial step of the

repair process as already observed in eukaryotes (26). However, reconstitution of the complete enzymatic process awaits further assessment.

ACKNOWLEDGEMENTS

We are grateful to Hannu Myllykallio for providing the expression clone encoding *Pab*RNase HII and critical reading of the manuscript. This work was financially supported by the French institute of marine research and exploitation (Ifremer). Sébastien Le Laz thanks the University of Western Brittany for funding.

REFERENCES

1. **Cann, I. K., K. Komori, H. Toh, S. Kanai, and Y. Ishino.** 1998. A heterodimeric DNA polymerase: evidence that members of Euryarchaeota possess a distinct DNA polymerase. Proc Natl Acad Sci U S A **95:**14250-5.
2. **Cerritelli, S. M., and R. J. Crouch.** 2009. Ribonuclease H: the enzymes in eukaryotes. Febs J **276:**1494-505.
3. **Chai, Q., J. Qiu, B. R. Chapados, and B. Shen.** 2001. *Archaeoglobus fulgidus* RNase HII in DNA replication: enzymological functions and activity regulation via metal cofactors. Biochem Biophys Res Commun **286:**1073-81.
4. **Chapados, B. R., Q. Chai, D. J. Hosfield, J. Qiu, B. Shen, and J. A. Tainer.** 2001. Structural biochemistry of a type 2 RNase H: RNA primer recognition and removal during DNA replication. J Mol Biol **307:**541-56.
5. **Chou, S. H., P. Flynn, and B. Reid.** 1989. Solid-phase synthesis and high-resolution NMR studies of two synthetic double-helical RNA dodecamers: r(CGCGAAUUCGCG) and r(CGCGUAUACGCG). Biochemistry **28:**2422-35.
6. **Cohen, G. N., V. Barbe, D. Flament, M. Galperin, R. Heilig, O. Lecompte, O. Poch, D. Prieur, J. Querellou, R. Ripp, J. C. Thierry, J. Van der Oost, J. Weissenbach, Y. Zivanovic, and P. Forterre.** 2003. An integrated analysis of the genome of the hyperthermophilic archaeon *Pyrococcus abyssi.* Mol Microbiol **47:**1495-512.
7. **Dickerson, R. E., H. R. Drew, B. N. Conner, R. M. Wing, A. V. Fratini, and M. L. Kopka.** 1982. The anatomy of A-, B-, and Z-DNA. Science **216:**475-85.
8. **Gueguen, Y., J. L. Rolland, O. Lecompte, P. Azam, G. Le Romancer, D. Flament, J. P. Raffin, and J. Dietrich.** 2001. Characterization of two DNA polymerases from the hyperthermophilic euryarchaeon *Pyrococcus abyssi*. Eur J Biochem **268:**5961-9.

9. **Haruki, M., K. Hayashi, T. Kochi, A. Muroya, Y. Koga, M. Morikawa, T. Imanaka, and S. Kanaya.** 1998. Gene cloning and characterization of recombinant RNase HII from a hyperthermophilic archaeon. J Bacteriol **180:**6207-14.

10. **Haruki, M., Y. Tsunaka, M. Morikawa, and S. Kanaya.** 2002. Cleavage of a DNA-RNA-DNA/DNA chimeric substrate containing a single ribonucleotide at the DNA-RNA junction with prokaryotic RNases HII. FEBS Lett **531:**204-8.

11. **Henneke, G., D. Flament, U. Hubscher, J. Querellou, and J. P. Raffin.** 2005. The hyperthermophilic euryarchaeota *Pyrococcus abyssi* likely requires the two DNA polymerases D and B for DNA replication. J Mol Biol **350:**53-64.

12. **Lai, L., H. Yokota, L. W. Hung, R. Kim, and S. H. Kim.** 2000. Crystal structure of archaeal RNase HII: a homologue of human major RNase H. Structure **8:**897-904.

13. **Lao-Sirieix, S. H., and S. D. Bell.** 2004. The heterodimeric primase of the hyperthermophilic archaeon *Sulfolobus solfataricus* possesses DNA and RNA primase, polymerase and 3'-terminal nucleotidyl transferase activities. J Mol Biol **344:**1251-63.

14. **Le Breton, M., G. Henneke, C. Norais, D. Flament, H. Myllykallio, J. Querellou, and J. P. Raffin.** 2007. The heterodimeric primase from the euryarchaeon *Pyrococcus abyssi:* a multifunctional enzyme for initiation and repair? J Mol Biol **374:**1172-85.

15. **Matsunaga, F., C. Norais, P. Forterre, and H. Myllykallio.** 2003. Identification of short 'eukaryotic' Okazaki fragments synthesized from a prokaryotic replication origin. EMBO Rep **4:**154-8.

16. **Meslet-Cladiere, L., C. Norais, J. Kuhn, J. Briffotaux, J. W. Sloostra, E. Ferrari, U. Hubscher, D. Flament, and H. Myllykallio.** 2007. A novel proteomic approach identifies new interaction partners for proliferating cell nuclear antigen. J Mol Biol **372:**1137-48.

17. **Murante, R. S., L. A. Henricksen, and R. A. Bambara.** 1998. Junction ribonuclease: an activity in Okazaki fragment processing. Proc Natl Acad Sci U S A **95:**2244-9.

18. **Murante, R. S., J. A. Rumbaugh, C. J. Barnes, J. R. Norton, and R. A. Bambara.** 1996. Calf RTH-1 nuclease can remove the initiator RNAs of Okazaki fragments by endonuclease activity. J Biol Chem **271:**25888-97.

19. **Muroya, A., D. Tsuchiya, M. Ishikawa, M. Haruki, M. Morikawa, S. Kanaya, and K. Morikawa.** 2001. Catalytic center of an archaeal type 2 ribonuclease H as revealed by X-ray crystallographic and mutational analyses. Protein Sci **10:**707-14.

20. **Nick McElhinny, S. A., B. E. Watts, D. Kumar, D. L. Watt, E. B. Lundstrom, P. M. Burgers, E. Johansson, A. Chabes, and T. A. Kunkel.** 2010. Abundant ribonucleotide incorporation into DNA by yeast replicative polymerases. Proc Natl Acad Sci U S A **107:**4949-54.

21. **Ohtani, N., M. Haruki, M. Morikawa, and S. Kanaya.** 1999. Molecular diversities of RNases H. J Biosci Bioeng **88:**12-9.

22. **Ohtani, N., M. Tomita, and M. Itaya.** 2008. Junction ribonuclease: a ribonuclease HII orthologue from *Thermus thermophilus* HB8 prefers the RNA-DNA junction to the RNA/DNA heteroduplex. Biochem J **412:**517-26.

23. **Ohtani, N., H. Yanagawa, M. Tomita, and M. Itaya.** 2004. Cleavage of double-stranded RNA by RNase HI from a thermoacidophilic archaeon, *Sulfolobus tokodaii* 7. Nucleic Acids Res **32:**5809-19.

24. **Ohtani, N., H. Yanagawa, M. Tomita, and M. Itaya.** 2004. Identification of the first archaeal Type 1 RNase H gene from *Halobacterium sp.* NRC-1: archaeal RNase HI can cleave an RNA-DNA junction. Biochem J **381:**795-802.

25. **Rouillon, C., G. Henneke, D. Flament, J. Querellou, and J. P. Raffin.** 2007. DNA polymerase switching on homotrimeric PCNA at the replication fork of the euryarchaea *Pyrococcus abyssi.* J Mol Biol **369:**343-55.

26. **Rumbaugh, J. A., R. S. Murante, S. Shi, and R. A. Bambara.** 1997. Creation and removal of embedded ribonucleotides in chromosomal DNA during mammalian Okazaki fragment processing. J Biol Chem **272:**22591-9.

27. **Sato, A., A. Kanai, M. Itaya, and M. Tomita.** 2003. Cooperative regulation for Okazaki fragment processing by RNase HII and FEN-1 purified from a hyperthermophilic archaeon, *Pyrococcus furiosus*. Biochem Biophys Res Commun **309:**247-52.

28. **Sheaff, R. J., and R. D. Kuchta.** 1994. Misincorporation of nucleotides by calf thymus DNA primase and elongation of primers containing multiple noncognate nucleotides by DNA polymerase alpha. J Biol Chem **269:**19225-31.

29. **Stein, H., and P. Hausen.** 1969. Enzyme from calf thymus degrading the RNA moiety of DNA-RNA Hybrids: effect on DNA-dependent RNA polymerase. Science **166:**393-5.

30. **Tadokoro, T., and S. Kanaya.** 2009. Ribonuclease H: molecular diversities, substrate binding domains, and catalytic mechanism of the prokaryotic enzymes. Febs J **276:**1482-93.

31. **Thomas, D. C., J. D. Roberts, R. D. Sabatino, T. W. Myers, C. K. Tan, K. M. Downey, A. G. So, R. A. Bambara, and T. A. Kunkel.** 1991. Fidelity of mammalian DNA replication and replicative DNA polymerases. Biochemistry **30:**11751-9.

32. **Von Sonntag, C., and D. Schulte-Frohlinde.** 1978. Radiation-induced degradation of the sugar in model compounds and in DNA. Mol Biol Biochem Biophys **27:**204-26.

501 **FIGURE LEGENDS**

502

503 **Fig. 1 Enzymatic properties of *Pab*RNase HII**. (A) Alignment of the amino acid sequences
504 of archaeal RNase HII homologues. Sequences are from the three euryarchaeota species, *P.*
505 *abyssi* (Pab, accession number, gi: 14520734), *T. kodakaraensis KOD1* (Tko, accession
506 number, gi: 57640740), *A. fulgidus* (Afu, accession number, gi: 11498229). Conserved amino
507 acid residues are shaded black. Similar amino acid residues are framed black. Proposed active
508 sites residues are indicated by asterisks. Secondary structure is shown above the sequences,
509 denoting β-sheets (arrows) and α-helices (ribbons). (B) SDS-PAGE gradient gel (4-20 %) of
510 purified, recombinant His_6-tagged *Pab*RNase HII (0.5 µg; lane 2) and molecular mass
511 markers (lane 1) stained with Coomassie Blue (C) pH dependence. The enzymatic activities
512 were determined at 60°C for 30 min in reaction buffer containing 50 mM Tris-HCl, 5 mM
513 dithiothreitol, 5 mM $MgCl_2$, 50 nM of *Pab*RNase HII and 50 nM of RNA-DNA/DNA
514 substrate (S1) with pH values ranging from 5 to 10. Data are the average of triplicate
515 measurements. (D) Divalent cation dependence. The enzymatic activities were determined at
516 60°C for 30 min in reaction buffer containing 50 mM Tris-HCl (pH 8), 5 mM dithiothreitol,
517 50 nM of *Pab*RNase HII and 50 nM of RNA-DNA/DNA substrate (S1) at the indicated
518 concentrations of $MgCl_2$ (◆), $MnCl_2$ (Δ) and $CoCl_2$ (■). Data are the average of triplicate
519 measurements.

520

521 **Fig. 2 Ribonuclease activity by *Pab*RNase HII.** (A) Indicated amounts of *Pab*RNase HII
522 were incubated with the S11 substrate (lanes 2-8) and a base-hydrolysed ladder (lane 1) was
523 prepared as described (see Materials and methods section). 5'-end fluorescently labelled
524 products were visualised with a Mode Imager Typhoon 9400 (GE Healthcare) and
525 quantification was performed using Image Quant 5.2 software. (B) *Pab*RNase HII was

incubated with the 32-base single-stranded RNA oligonucleotide at the indicated amounts (lanes 1-4). An 8-nt RNA oligonucleotide was used as a ladder (lane 5). 5'-end fluorescently labelled products were visualised with a Mode Imager Typhoon 9400 (GE Healthcare).

Fig. 3 *Pab*RNaseHII specifically cleaves RNA-initiated DNA segments fully annealed to a DNA template. (A) Substrate structure representations of S1, S2, and S3. The thick line and the closed circle represent the RNA portion and the fluorescent label, respectively. (B) Indicated amounts of *Pab*RNase HII were incubated with S1 substrate (lanes 2-5), S2 substrate (lanes 6-9) and S3 substrate (lanes 10-13). A base-hydrolysed ladder (lane 1) was prepared as explained in the Materials and methods section. Fluorescent-labelled products were visualised with a Mode Imager Typhoon 9400 (GE Healthcare) and quantification was performed using Image Quant 5.2 software.

Fig. 4 *Pab*RNase HII specifically cleaves the fully annealed RNA strand of Okazaki fragment-gapped intermediates but not a 5'-RNA flap. (A) Substrate structure representations of S4, S5, and S6. The thick line and the closed circle represent the RNA portion and the fluorescent label, respectively. (B) Indicated amounts of *Pab*RNase HII were incubated with S4 substrate (lanes 1-4), S5 substrate (lanes 5-8) and S6 substrate (lanes 9-12). An 18-nt nucleotide was used as an appropriate ladder (lane 13). Fluorescent-labelled products were visualised with a Mode Imager Typhoon 9400 (GE Healthcare) and quantification was performed using Image Quant 5.2 software.

Fig. 5 *Pab*RNase HII specifically cuts the RNA-DNA/DNA when the RNA is completely annealed to the DNA template. (A) Substrate structure representations of S7, S8, and S9. The thick line and the closed circle represent the RNA portion and the fluorescent label,

551 respectively. (B) Indicated amounts of *Pab*RNase HII were incubated with S7 substrate (lanes
552 2-5), S8 substrate (lanes 6-9) and S9 substrate (lanes 10-13). An 11-nt nucleotide was used as
553 an appropriate ladder (lane 1). Fluorescent-labelled products were visualised with a Mode
554 Imager Typhoon 9400 (GE Healthcare) and quantification was performed using Image Quant
555 5.2 software. (C) Graphical representation of sites and extents of cleavage in mismatches
556 RNA-DNA/DNA substrates. Cleavage sites are denoted by different bars.
557 Deoxyribonucleotides and ribonucleotides are shown by uppercase and lowercase letters,
558 respectively.
559
560 **Fig. 6 *Pab*RNase HII specifically cuts single embedded ribonucleotide in a DNA duplex.**
561 (A) Substrate structure representations of S1 and S10. The thick line and the closed circle
562 represent the RNA portion and the fluorescent label, respectively. (B) Indicated amounts of
563 *Pab*RNase HII were incubated with S1 substrate (lanes 2-5) and S10 substrate (lanes 8-11).
564 Both substrates and the corresponding hydrolysed products were manually labelled. Lanes 1
565 and 6 are appropriate 11-nt and 12-nt ladders for hydrolysed S1 substrates. Lanes 7 and 12 are
566 suitable 11-nt and 12-nt ladders for hydrolysed S10 substrates. Fluorescent-labelled products
567 were visualised with a Mode Imager Typhoon 9400 (GE Healthcare) and quantification was
568 performed using Image Quant 5.2 software.
569
570 **TABLE 1 Oligonucleotide sequences used to create structural duplex substrates**
571 S1 substrate comprises primers 2 and template 8; S2 substrate is primer 2; S3 substrate
572 comprises primers 2 and template 8; S4 substrate consists of primers 2, 3 and template 7; S5
573 substrate contains primers 2, 4 and template 7; S6 substrate includes primers 2, 5 and template
574 9; S7 substrate consists of primer 2 and template 12; S8 substrate is composed of primer 2 and
575 template 11; S9 substrate consists of primer 2 and template 10; S10 substrate comprises

primer 6 and template 8; S11 substrate contains primer 1 and template 7. Deoxyribonucleotides and ribonucleotides are shown by uppercase and lowercase letters, respectively.

TABLE 2 Kinetic parameters of archaeal RNase HII. Hydrolyses of RNA-DNA/DNA substrates (S1) were carried out at 60°C in *Pab*RNase HII reaction buffer as described in the Materials and methods section. The data were fit by nonlinear regression using the Marquardt-Levenberg algorithm (EnzFitter 2.0, BioSoft) to the Michaelis-Menten equation. Kinetic parameters, K_m and V_{max}, obtained from the fit were used to calculate the catalytic efficiency (k_{cat}/K_m) of *Pab*RNase HII. The kinetics values are the average of at least triplicate determinations and are shown with standard deviations (SD). Kinetic parameters of *Afu*RNase HII were extracted from previous studies (4).

A

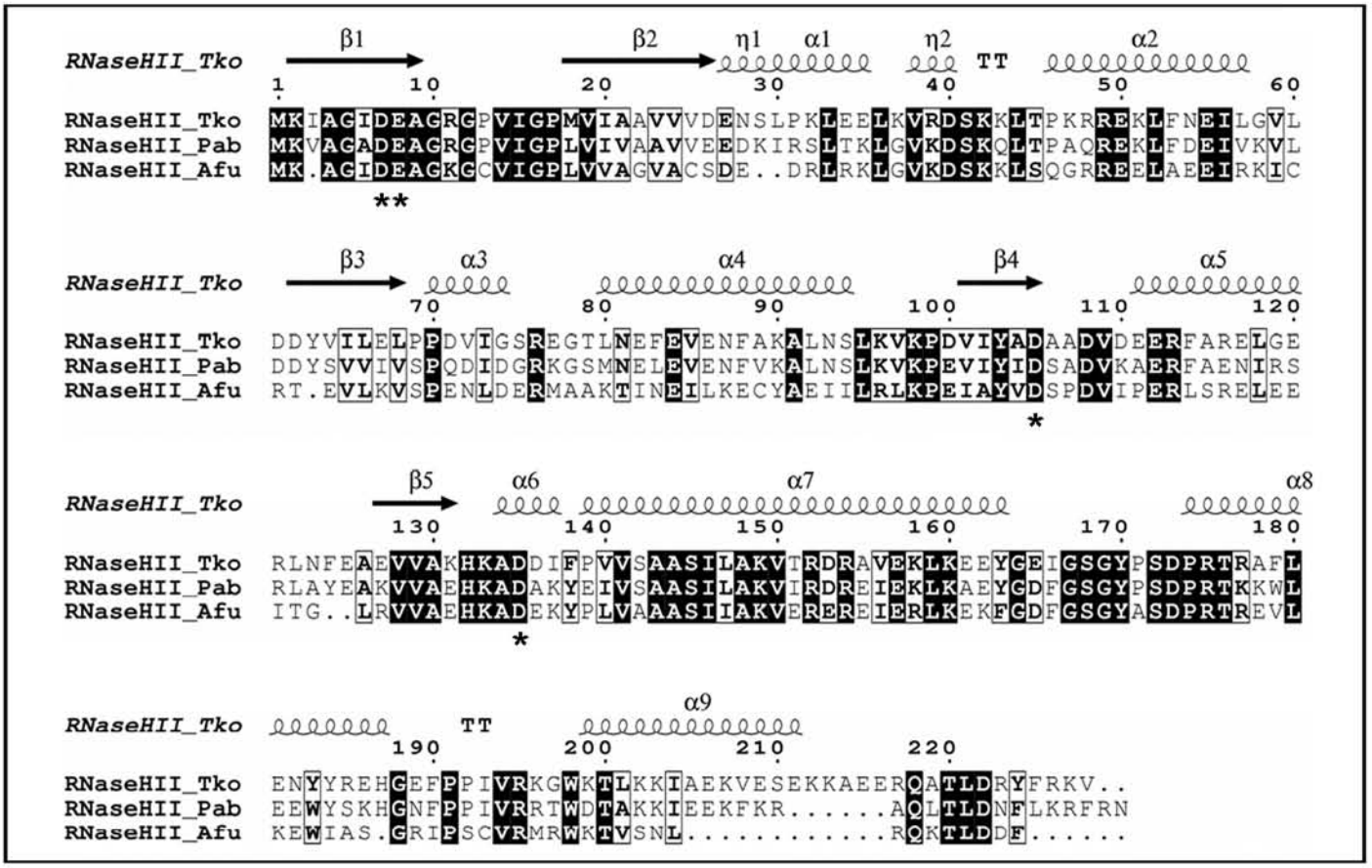
β1 β2 η1 α1 η2 α2
RNaseHII_Tko
1 10 20 30 40 50 60
RNaseHII_Tko MKIAGIDEAGRGPVIGPMVIAAVVVDENSLPKLEELKVRDSKKLTPKRREKLFNEILGVL
RNaseHII_Pab MKVAGADEAGRGPVIGPLVIVAAVVEEDKIRSLTKLGVKDSKQLTPAQREKLFDEIVKVL
RNaseHII_Afu MK.AGIDEAGKGCVIGPLVVAGVACSDE..DRLRKLGVKDSKKLSQGRREELAEEIRKIC
β3 α3 α4 β4 α5
RNaseHII_Tko
70 80 90 100 110 120
RNaseHII_Tko DDYVILELPPDVIGSREGTLNEFEVENFAKALNSLKVKPDVIYADAADVDEERFARELGE
RNaseHII_Pab DDYSVVIVSPQDIDGRKGSMNELEVENFVKALNSLKVKPEVIYIDSADVKAERFAENIRS
RNaseHII_Afu RT.EVLKVSPENLDERMAAKTINEILKECYAEIILRLKPEIAYVDSPDVIPERLSRELEE
β5 α6 α7 α8
RNaseHII_Tko
130 140 150 160 170 180
RNaseHII_Tko RLNFEAEVVAKHKADDIFPVVSAASILAKVTRDRAVEKLKEEYGEIGSGYPSDPRTRAFL
RNaseHII_Pab RLAYEAKVVAEHKADAKYEIVSAASILAKVIRDREIEKLKAEYGDFGSGYPSDPRTKKWL
RNaseHII_Afu ITG..LRVVAEHKADEKYPLVAAASIIAKVERERIERLKEKFGDFGSGYASDPRTREVL
α9
RNaseHII_Tko TT
190 200 210 220
RNaseHII_Tko ENYYREHGEFPPIVRKGWKTLKKIAEKVESEKKAEERQATLDRYFRKV..
RNaseHII_Pab EEWYSKHGNFPPIVRRTWDTAKKIEEKFKR.....AQLTLDNFLKRFRN
RNaseHII_Afu KEWIAS.GRIPSCVRMRWKTVSNL.....RQKTLDDF.....

B

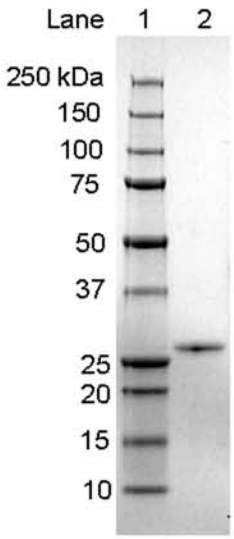
Lane 1 2
250 kDa
150
100
75
50
37
25
20
15
10

Fig. 1

C

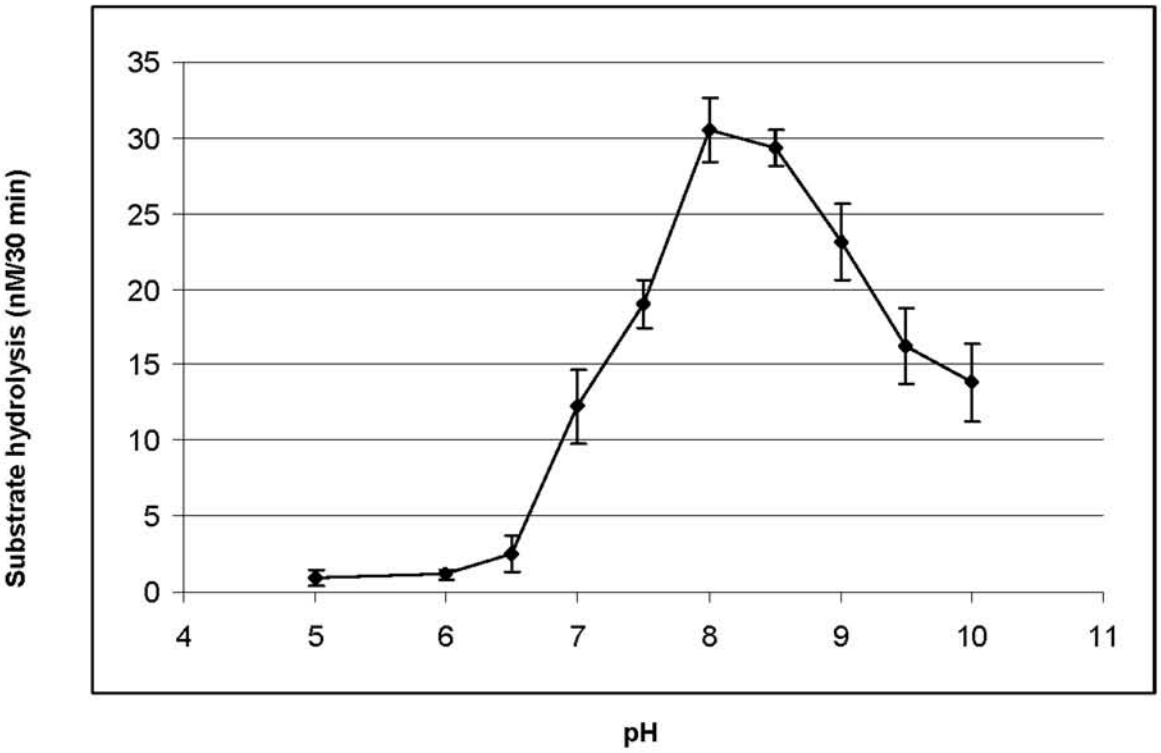
Substrate hydrolysis (nM/30 min)
35
30
25
20
15
10
5
0
4
5
6
7
8
9
10
11
pH

D

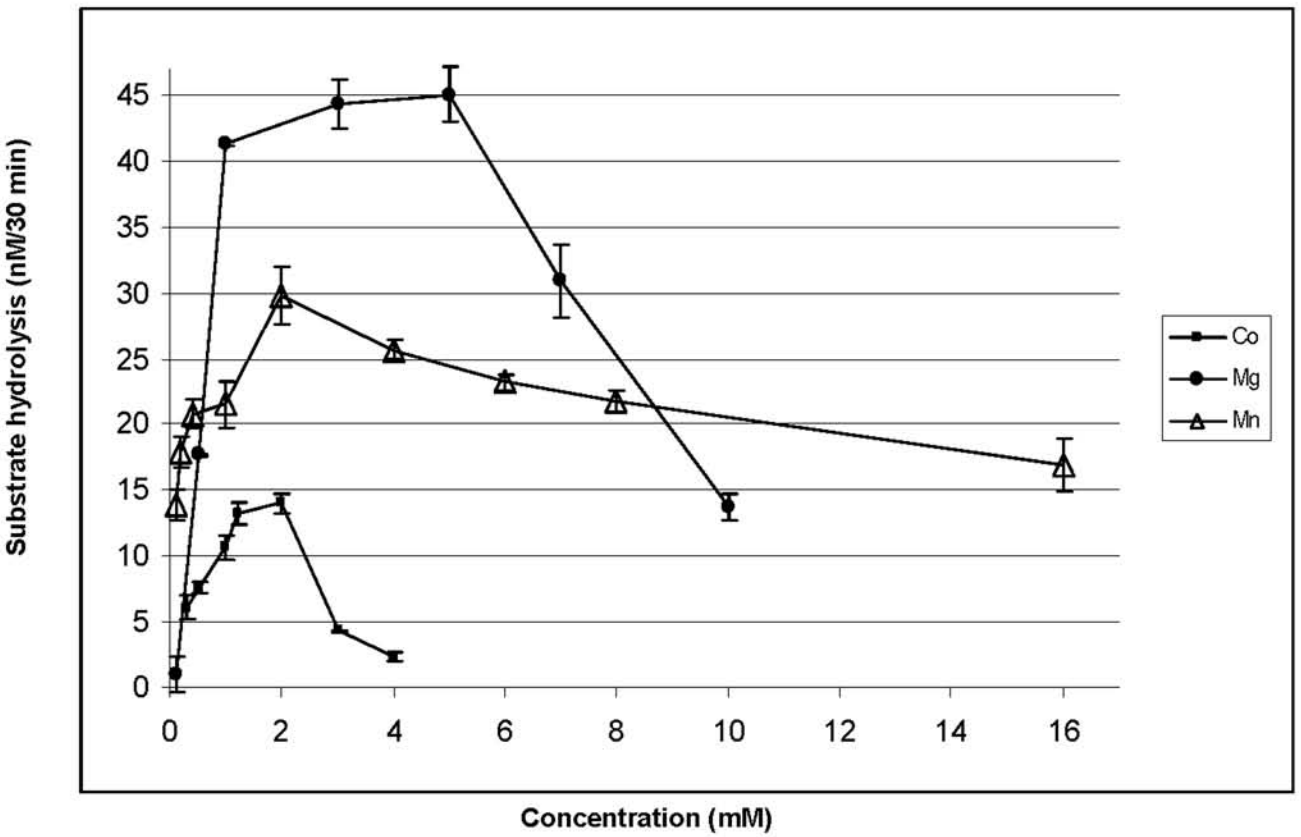
Substrate hydrolysis (nM/30 min)
45
40
35
30
25
20
15
10
5
0
0
2
4
6
8
10
12
14
16
Concentration (mM)
Co
Mg
Mn

Fig. 1

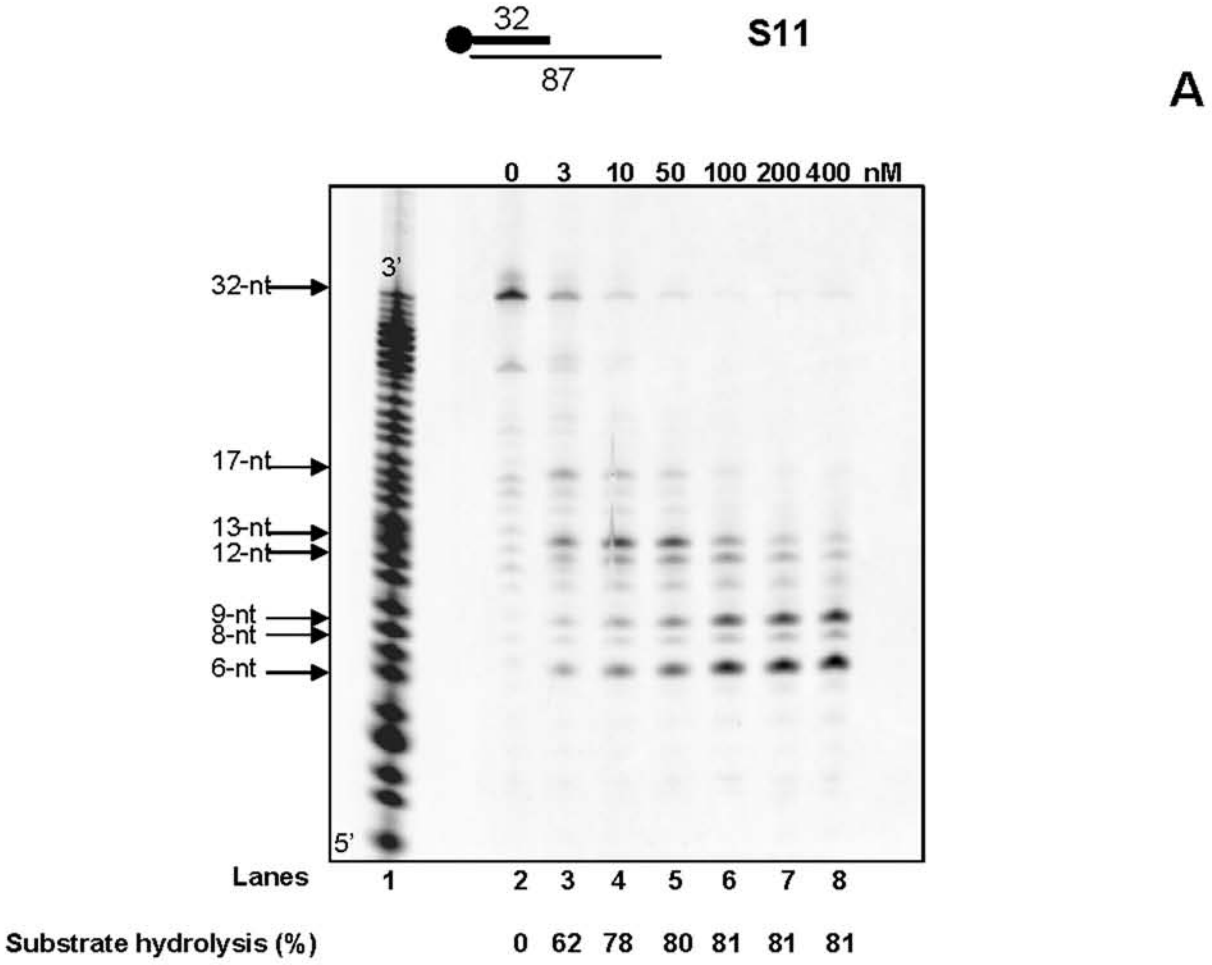
32
87
S11
A
0 3 10 50 100 200 400 nM
3'
32-nt
17-nt
13-nt
12-nt
9-nt
8-nt
6-nt
5'
Lanes
1 2 3 4 5 6 7 8
Substrate hydrolysis (%)
0 62 78 80 81 81 81
B
32
0 10 100 1000 nM
32-nt
8-nt
Lanes
1 2 3 4 5

Fig. 2

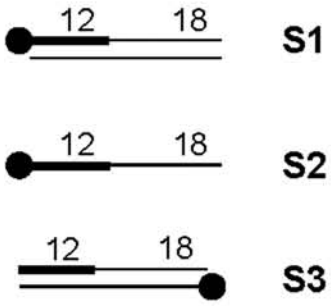
12
18
S1
12
18
S2
12
18
S3

A

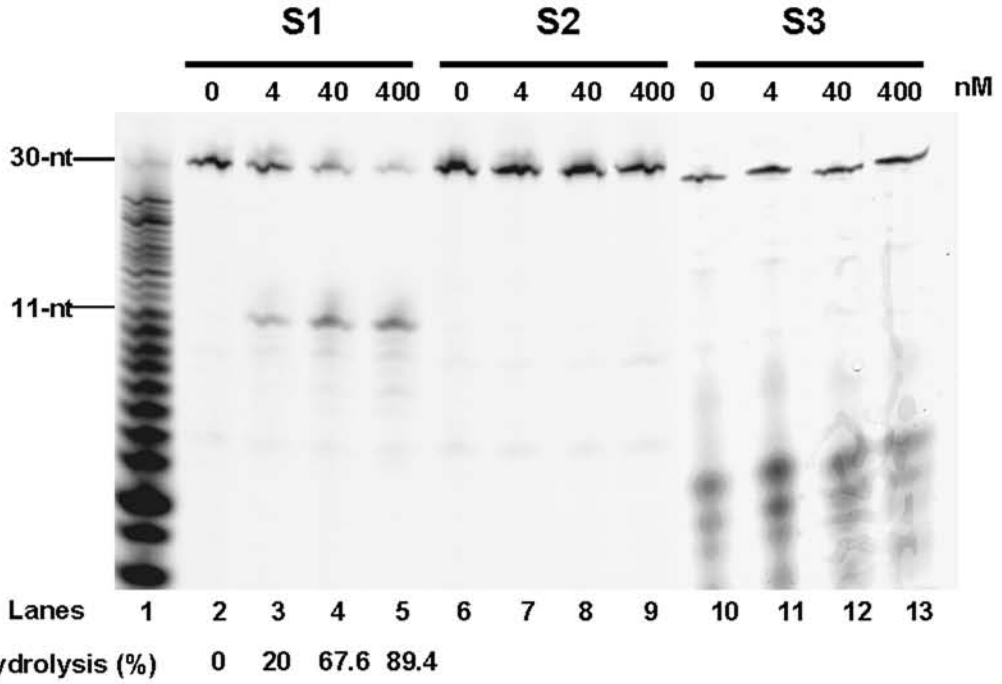
S1
S2
S3
0 4 40 400 0 4 40 400 0 4 40 400 nM
30-nt
11-nt
Lanes 1 2 3 4 5 6 7 8 9 10 11 12 13
Substrate hydrolysis (%) 0 20 67.6 89.4

B

Fig. 3

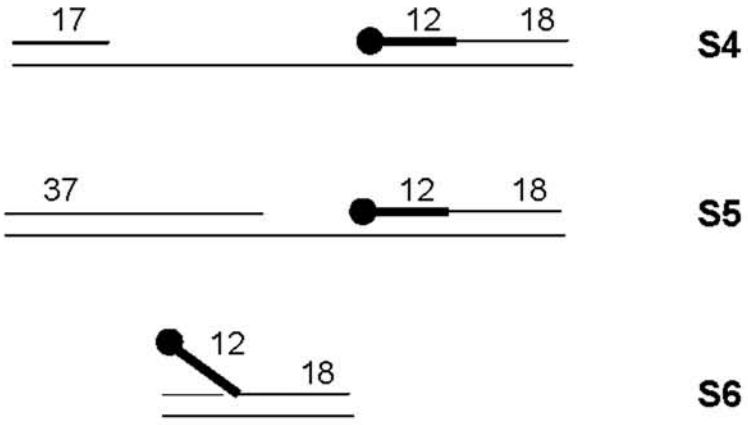
17
12
18
S4
37
12
18
S5
12
18
S6

A

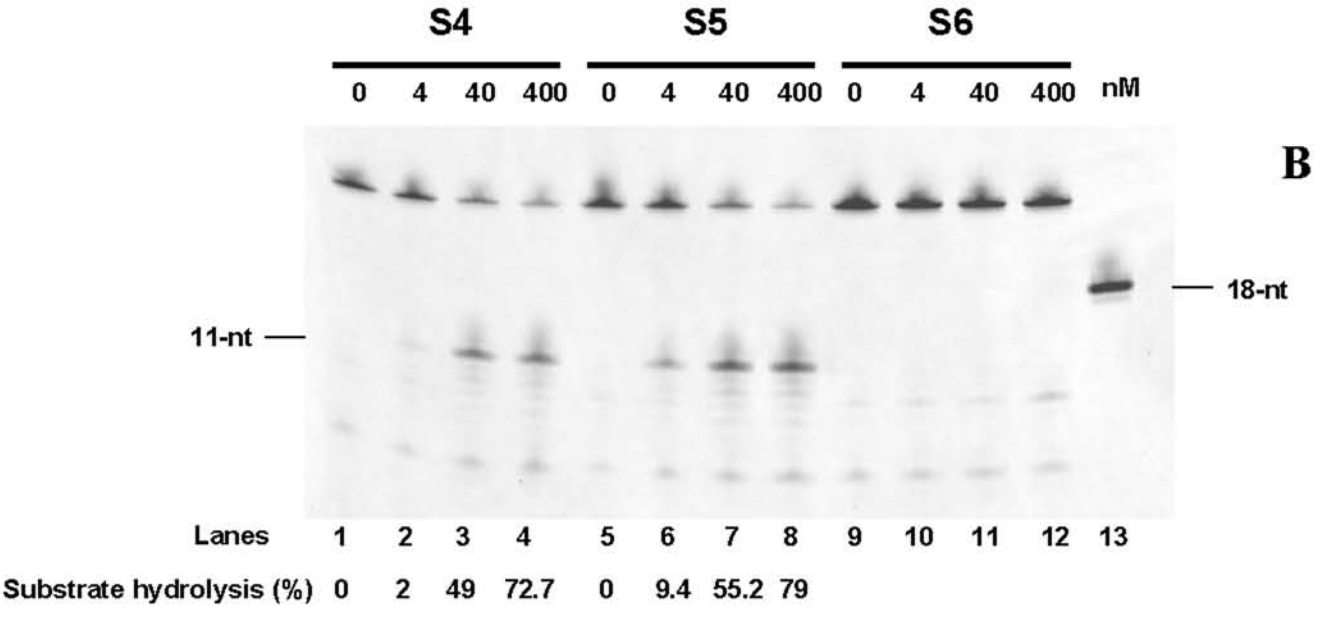
S4
S5
S6
0 4 40 400 0 4 40 400 0 4 40 400 nM
11-nt
18-nt
Lanes 1 2 3 4 5 6 7 8 9 10 11 12 13
Substrate hydrolysis (%) 0 2 49 72.7 0 9.4 55.2 79

B

Fig. 4

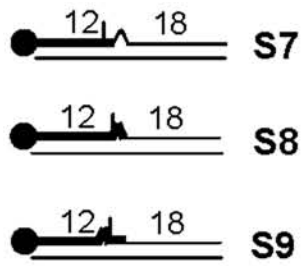
12
18
S7
12
18
S8
12
18
S9

A

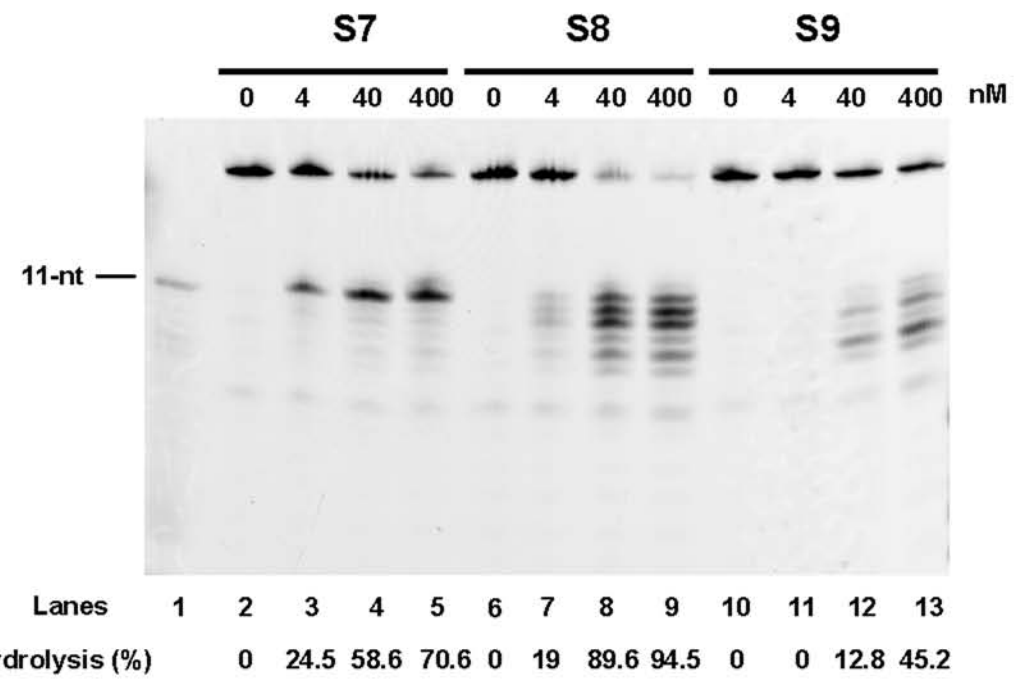
S7
S8
S9
0 4 40 400 0 4 40 400 0 4 40 400 nM
11-nt
B
Lanes 1 2 3 4 5 6 7 8 9 10 11 12 13
Substrate hydrolysis (%) 0 24.5 58.6 70.6 0 19 89.6 94.5 0 0 12.8 45.2

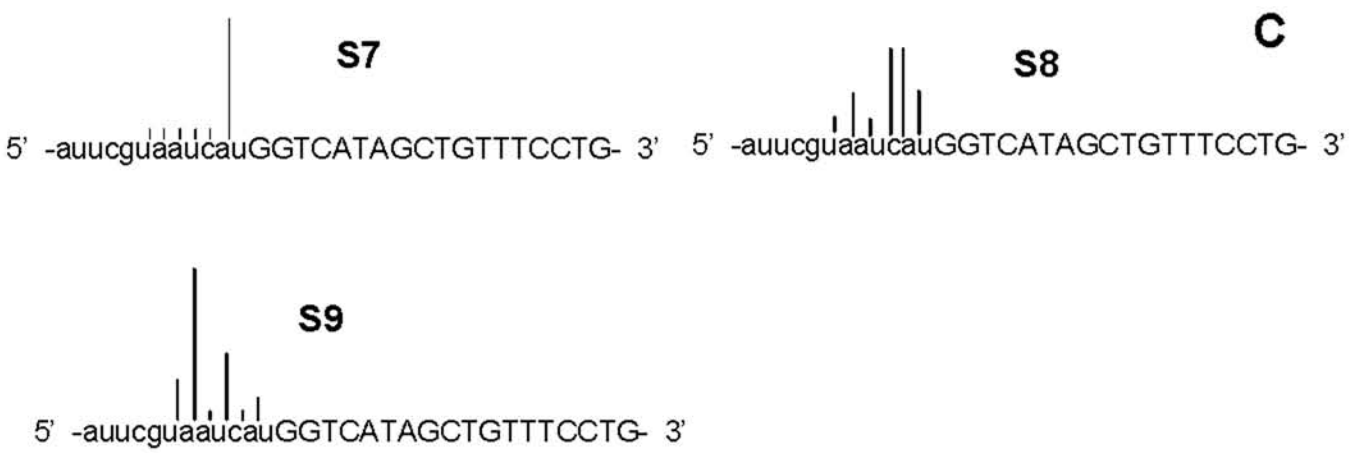
C
S7
5' -auucguaaucauGGTCATAGCTGTTTCCTG- 3'
S8
5' -auucguaaucauGGTCATAGCTGTTTCCTG- 3'
S9
5' -auucguaaucauGGTCATAGCTGTTTCCTG- 3'

Fig. 5

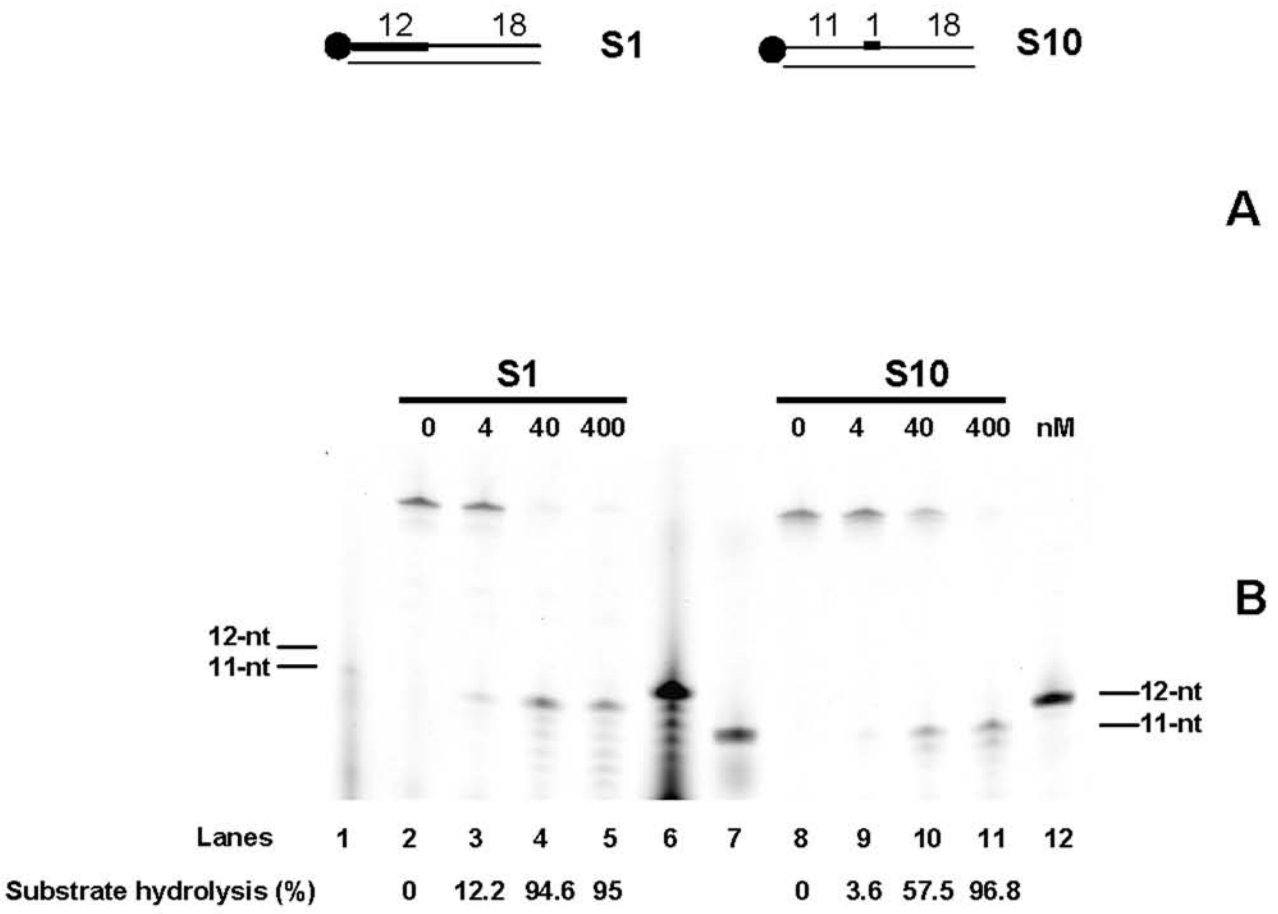
12
18
S1
11
1
18
S10
A
S1
S10
0
4
40
400
0
4
40
400
nM
B
12-nt
11-nt
12-nt
11-nt
Lanes
1
2
3
4
5
6
7
8
9
10
11
12
Substrate hydrolysis (%)
0
12.2
94.6
95
0
3.6
57.5
96.8

Fig. 6

Primers	Length	Sequence
1	32-nt	**ugccaagcuugcaugccugcaggucgacucua**
2	30-nt	**auucguaaucauGGTCATAGCTGTTTCCTG**
3	17-nt	**TGCCAAGCTTGCATGCC**
4	37-nt	**TGCCAAGCTTGCATGCCTGCAGGTCGACTCTAGAGGA**
5	12-nt	**TGGGTGGGGTGG**
6	30-nt	**ATTCGTAATCAuGGTCATAGCTGTTTCCTG**
Templates	**Length**	**Sequence**
7	87-nt	**CAGGAAACAGCTATGACCATGATTACGAATTCGAGCTCGGTACCCGGGGATCCTCTAGAGTCGACCTGCAGGCATG CAAGCTTGGCA**
8	30-nt	**CAGGAAACAGCTATGACCATGATTACGAAT**
9	30-nt	**CAGGAAACAGCTATGACCCCACCCCACCCA**
10	30-nt	**CAGGAAACAGCTATGACCAGGATTACGAAT**
11	30-nt	**CAGGAAACAGCTATGACCGTGATTACGAAT**
12	30-nt	**CAGGAAACAGCTATGACTATGATTACGAAT**

Table1

Enzymes	K_m (μM)	k_{cat} (min^{-1})	k_{cat}/K_m
*Pab*RNase HII	0.50±0.15	5.57±0.54	11.14
*Afu*RNase HII	0.06±0.15	8.0±0.23	133.3

Table 2